
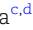




Typical and disrupted small-world architecture and regional communication in full-term and preterm infants

Huiqing Hu ^{a,b}, Peter Coppola ^{c,d}, Emmanuel A Stamatakis ^{c,d} and Lorina Naci ^{e,f,*}

^aKey Laboratory of Adolescent Cyberpsychology and Behavior, Ministry of Education, Central China Normal University, No. 152 Luoyu Road, Hongshan District, Wuhan 430079, Hubei, China

^bKey Laboratory of Human Development and Mental Health of Hubei Province, School of Psychology, Central China Normal University, No. 152 Luoyu Road, Hongshan District, Wuhan 430079, Hubei, China

^cDivision of Anaesthesia, Addenbrookes Hospital, University of Cambridge, Hills Rd, Cambridge CB2 0QQ, United Kingdom

^dDepartment of Psychology, University of Cambridge, Downing Street, Cambridge CB2 3EB, United Kingdom

^eTrinity College Institute of Neuroscience, School of Psychology, Trinity College Dublin, 42a Pearse St, Dublin D02 X9W9, Ireland

^fGlobal Brain Health Institute, Trinity College Dublin, 42a Pearse St, Dublin D02 X9W9, Ireland

*To whom correspondence should be addressed: Email: nacil@tcd.ie

Edited By Stephen Fleming

Abstract

Understanding the emergence of complex cognition in the neonate is one of the great frontiers of cognitive neuroscience. In the adult brain, small-world organization enables efficient information segregation and integration and dynamic adaptability to cognitive demands. It remains unknown, however, when functional small-world architecture emerges in development, whether it is present by birth and how prematurity affects it. We leveraged the world's largest fMRI neonatal dataset—Developing Human Connectome Project—to include full-term neonates ($n = 278$), and preterm neonates scanned at term-equivalent age (TEA; $n = 72$), or before TEA ($n = 70$), and the Human Connectome Project for a reference adult group ($n = 176$). Although different from adults', the small-world architecture was developed in full-term neonates at birth. The key novel finding was that premature neonates before TEA showed dramatic underdevelopment of small-world organization and regional communication in 9/11 networks, with disruption in 32% of brain nodes. The somatomotor and dorsal attention networks carry the largest spatial effect, and visual network the smallest. Significant prematurity-related disruption of small-world architecture and reduced efficiency of regional communication in networks related to high-order cognition, including language, persisted at TEA. Critically, at full-term birth or by TEA, infants exhibited functional small-world architecture, which facilitates differentiated and integrated neural processes that support complex cognition. Conversely, this brain infrastructure is significantly underdeveloped before infants reach TEA. These findings improve understanding of the ontogeny of functional small-world architecture and efficiency of neural communication, and of their disruption by premature birth.

Keywords: neonate, premature birth, small-world architecture, regional communication, functional magnetic resonance imaging

Significance Statement

The brain's functional small-world organization supports complex cognition, but its development at birth remains unknown. Leveraging the world's largest neonatal functional MRI dataset, we investigated the impact of prematurity and neonatal age on small-world architecture and regional communication efficiency. Our results show that, premature neonates before term-equivalent age (TEA) have significantly weaker small-world organization and lower neural integration than full-term born counterparts. The somatomotor and dorsal attention networks carry the largest spatial effect, and the visual network the smallest. Despite persisting, significant prematurity-related disruption in very few regions, a preprogrammed developmental trajectory of functional architecture unfolds regardless of prematurity, as premature infants reach TEA. Results shed light on the ontogeny of functional small-world architecture in the infant brain.

Introduction

Understanding the emergence of complex cognition in the infant brain is one of the great frontiers of cognitive neuroscience. The development of brain infrastructural features that support complex cognition in adults, such as the presence of distinct brain networks and “small-world” organization, are key for understanding the capacity for and emergence time-course of cognitive faculties

in the neonate. Recent well-powered and methodologically rigorous infant studies have broken new ground in understanding the ontogeny of brain networks (1–7). For example, using the largest dataset of infant neuroimaging, from the Developing Human Connectome Project (dHCP), Eyre et al. (4) reported an adult-like topography in sensorimotor, visual, auditory, language, and ocular control networks. Using the same dataset, Hu et al. (2) detected

Competing Interest: The authors declare no competing interests.

Received: May 15, 2024. **Accepted:** January 3, 2025

© The Author(s) 2025. Published by Oxford University Press on behalf of National Academy of Sciences. This is an Open Access article distributed under the terms of the Creative Commons Attribution-NonCommercial License (<https://creativecommons.org/licenses/by-nc/4.0/>), which permits non-commercial re-use, distribution, and reproduction in any medium, provided the original work is properly cited.

the presence of distinct high-order networks, particularly the default mode network (DMN), dorsal attention network (DAN), and executive control network (ECN), as well as of the reciprocal relationship between the DMN and DAN by birth, in full-term born neonates and neonates born prematurely when they reached term-equivalent age (TEA) (postmenstrual age [PMA] of 37 weeks), but not prior to this age.

By contrast, little is known on whether small-world organization is present by birth and how it is affected by prematurity. Through dense within-network connections that facilitate specialized processes and sparse between-network connections that enhance global information integration (8, 9), small-world organization of adult brain networks (8, 10) balances segregation and integration of neural representations. Small-world organization in adults has been shown to enable rapid and efficient information transfer and processing (11–14), the dynamic adaptability to cognitive demands, and maintenance of cognitive performance across various tasks and conditions (8, 15, 16). Stronger functional small-world architecture has been associated with higher intelligence quotient (17, 18) and better cognitive performance (19). The opposite pattern of results has been observed during memory encoding and recognition in older compared to young adults (20). Furthermore, small-world organization is modulated by consciousness state manipulations across widely different conditions, i.e. sleep, anesthesia (21, 22), and brain injury (23, 24), further suggesting that small-world organization supports complex cognition that is disrupted by these whole-brain state manipulations.

Thus, understanding the development of small-world architecture can elucidate not only the ontogeny of brain development but also whether the capacity for complex cognition, that this architecture supports, is present within the first days of life. A literature search in PubMed with keywords “small-world architecture” or “small worldness” or “small-world propensity,” “infant” or “newborn” or “neonate” and “fMRI” or “functional imaging,” revealed very few studies delivering inconsistent findings (Table 1). A handful have suggested that the small-world architecture is present in full-term born neonates [Table 1 (25–29)], but the index (σ) (30) used to quantify small-world properties in these studies has been criticized (9, 11, 31), due to a high false-positive rate (31). In addition, the small sample size ($n = 10$ to 66) and low temporal and spatial resolution limit their results’ reliability. The effects of premature birth on small-world organization has, to the best of our knowledge, been investigated only in four studies examining neonates at TEA (PMA of 37 weeks) [Table 1 (25, 26)], and two studies of neonates before TEA [Table 1 (28, 32)], with very small samples ($n = 11$ to 66). These studies have offered inconsistent results, including stronger, weaker or no difference in small worldness due to prematurity, likely due to different neuroimaging techniques, different brain atlases, and very small sample sizes.

Furthermore, a big gap remains in understanding of the effect of prematurity on integration and segregation at the brain regional level in neonates, especially given the varying developmental rates of different brain regions. For example, Doria et al. (33) observed medial visual, auditory, somatosensory, motor, cerebellum, brainstem, and thalamic and default mode in neonates at 30 weeks of age, but not lateral visual, dorsal visual stream, ECN until 34 weeks of age. The interhemispheric connectivity in motor, somatosensory, DMN, and ECN increased with increasing age from 28 to 44 weeks of age, whereas that of the visual cortex decreased with increasing age. Before TEA, the DAN is present in preterm neonates, while the default mode network and executive network are dramatically underdeveloped at this time (2).

Premature birth, in and of itself, has also been associated with differential atypical development of functional architecture within and across brain networks (2, 4, 6, 34). However, the effects of early age and prematurity have not been dissociated in previous studies.

To address these gaps, we first investigated whether small-world organization was developed at birth, and how it was affected by prematurity and neonate age across the brain. We then asked how the balance of segregation and integration at the regional level were affected by premature birth and neonate age. To address the limitations of previous studies, we used rs-fMRI data from the largest open-source neonate dataset, the dHCP, which conferred several advantages, including a large sample size ($n = 278$), 3T MRI multiband echo-planar imaging (EPI), that significantly improves temporal resolution and signal-to-noise ratio relative to sequences used in previous studies (35), registration to more accurate week-to-week neonate structural templates, and significant improvements in motion correction (see Materials and methods for further details). We also included a large reference adult group ($n = 176$) from the Human Connectome Project (HCP). The effect of chronological age at the time of assessment was deconfounded from the effect of premature birth (36) by the inclusion of two groups: the first ($n = 72$) born before and scanned at TEA, and the second ($n = 70$) born and scanned before TEA. A subset of paired scans collected from the same infants ($n = 33$) both before, and at TEA, was also included. We reasoned that any differences between neonates born and scanned at full-term and preterm neonates scanned at TEA would reflect the effects of premature birth, while controlling for neonate age. Conversely, any differences between preterm neonates scanned at TEA and those scanned before TEA would reflect the effects of neonate age, while controlling for premature birth. The balance of segregation and integration was assessed with rigorous measures of small-world architecture (37) across the brain, and with measures of nodal efficiency (38) at the regional level. Based on our previous work on the effects of premature birth on the development of high-order brain networks (2), we tested the following hypotheses: (i) small-world organization would be developed at birth, (ii) relative to full-term birth, premature birth would be associated with altered small-world architecture and nodal efficiency, and (iii) that some alterations in these measures would persist as preterm neonates reached TEA.

Results

Comparison of neonate and adult functional small-world architecture

The global scale network efficiency was measured using small-world propensity (ϕ) and its underlying measures (clustering coefficient and path length), and nodal scale communication efficiency was measured via nodal efficiency. The (ϕ) index proposed by Muldoon et al. (37) is used as a rigorous measure of small worldness that takes into account variations in network density and connection strengths (for the full description of this and merits relative to previously used metrics see section Small-world properties in Materials and methods).

General linear models (GLMs) comparing the adults and full-term neonates, including head motion and mean functional connectivity (FC) as covariates, showed significant main effects of groups for ϕ [$F(1, 450) = 74.69, P < 0.0001$] and normalized clustering coefficient (Δ_C) [$F(1, 450) = 167.78, P < 0.0001$], which was driven by significantly higher ϕ and lower Δ_C in the adults relative to

Table 1. A summary of functional imaging studies that investigated the development of small-world architecture in neonates.

Technique	Studies	Participants	Age at scan (PMA, weeks)	State during scan	Scanner	Network type	Atlas	Thresholds	Main findings
fMRI	Argyropoulou et al. (2022)	10 preterm at TEA	46.9 ± 7.2	Under sedation	1.5 T	B	UNC	0.15	$\sigma > 1$
		10 preterm at TEA	52.3 ± 10.1						
	Bouyssi-Kobar et al. (2019)	66 preterm at TEA	40.2 ± 1.6	Unsedated	3 T	B	AAL	0.18:0.01:0.48	$\sigma > 1$ γ : full-term > preterm
		66 full-term	41.1 ± 1.1						λ : full-term < preterm
	Gozdas et al. (2018)	24 preterm at TEA 51 full-term	39 – 41 40 – 42	Unsedated	3 T	B	AAL	0.06:0.01:0.3	σ : preterm > full-term
	Cao et al. (2017) Asis-Cruz et al. (2015) Fransson et al. (2011) Gao et al. (2011)	40 full-term and preterm	31.3 – 41.7	Unsedated	3 T	B & W	Voxelwise	0.05	$\sigma > 1$
		60 full-term	41.79 ± 0.86*	Unsedated	3 T	B	UNC	0.0:0.025:0.45	$\sigma > 1$
		18 full-term	40.5 ± 0.6	Unsedated	1.5 T	B	Voxelwise	0.2:0.05:0.4	$\sigma > 1$
		51 full-term and preterm	43.3 ± 1.7*	Unsedated	3 T	W	AAL	highest 1–50% according to P-value	$\sigma > 1$ γ increase with age λ decrease with age
	EEG	Omidvarnia et al. (2014)	11 preterm before TEA 10 full-term	- -	Unsedated	-	W	Data-specific atlas	0.05

The first column shows what functional imaging technique the study used. The second column shows a reference to the study. The fourth column shows the neonates' age at scan in postmenstrual weeks for studies without an asterisk and postbirth weeks plus 40 for studies with an asterisk. $\sigma > 1$ indicates that the neonate's brains exhibit a strong small-world architecture. AAL, automated anatomical labelling atlas; B, binary; PMA, postmenstrual age in weeks; W, weighted; σ , small worldness; γ , normalized clustering coefficient; λ , normalized characteristic path length.

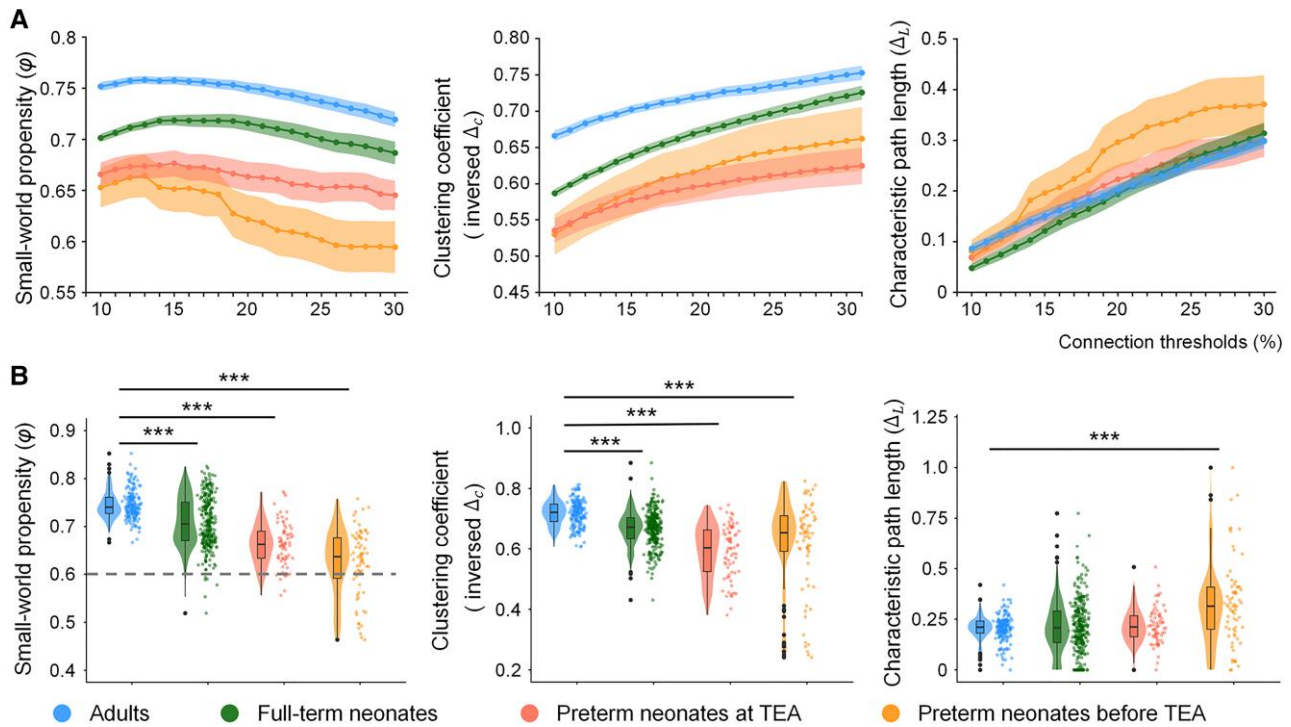


Fig. 1. The development of small-world architecture in the neonates relative to adults. A) Small-world properties at all tested thresholds (from 10 to 30% in 1% increments) and (B) small-world properties in the neonate groups relative to adults. The shaded areas shown in (a) represent the 95% CI. A) Network properties varied at different thresholds applied. Adults consistently exhibit higher small-world propensity and higher clustering coefficient relative to the three neonate groups at all 21 thresholds. Adults also showed lower characteristic path length relative to preterm neonates before TEA at 17/21 thresholds. To ensure that results were not driven by a specific choice of thresholds, the small-world propensity, clustering coefficient, and characteristic path length were averaged across 21 thresholds. Higher ϕ /inversed Δ_c/Δ_L represent higher small-world propensity, higher clustering coefficient and longer characteristic path length. The inversed Δ_c was calculated by $1 - \Delta_c$ and for visualization purposes only and the statistical analyses were conducted using Δ_c . B) The violin plots show the distribution of the data. The line that divides the box into two parts represents the median of the data. The ends of the box represent the upper (Q3) and lower (Q1) quartiles of the data. The extreme lines of the boxplot show $Q3 + 1.5 \cdot \text{interquartile}$ to $Q1 - 1.5 \cdot \text{interquartile}$ range. The black dots beyond the extreme lines show potential outliers. The gray dotted line represents the threshold of $\phi \geq 0.6$ used for identifying whether individuals exhibit a strong small-world architecture. TEA, term-equivalent age. *** $P < 0.0005$.

full-term neonates, respectively (Fig. 1B). We observed similar results when comparing the adults and preterm neonate groups. For preterm neonates scanned at TEA, we found significant main effects of group for ϕ [$F(1, 244) = 184.98, P < 0.0001$] and Δ_c [$F(1, 244) = 141.69, P < 0.0001$]. The adults had significantly higher ϕ and lower Δ_c relative to preterm neonates at TEA (Fig. 1B). Similarly, for the preterm neonates before TEA, we found significant main effects of group for ϕ [$F(1, 242) = 256.97, P < 0.0001$], and Δ_c [$F(1, 242) = 32.43, P < 0.0001$], which were driven by significantly higher ϕ and lower Δ_c in the adults (Fig. 1B). In addition, we observed a significant main effect for normalized path length (Δ_L) [$F(1, 242) = 53.78, P < 0.0001$], which was driven by significantly lower Δ_L in the adults. In summary, as expected, significantly higher small-world propensity/small worldness and clustering coefficient were consistently observed in the adult relative to neonate groups using different algorithms, types of FC matrices (Fig. S6) and brain parcellations (Fig. S7), which controlled for differences in FC and head motion between adult and infant groups.

Small-world organization in neonates

When a threshold value of $\phi \geq 0.6$ (37) was applied to detect whether neonates exhibited small-world architecture or not, the threshold was met or surpassed in 100% of the adults, 97.8% of full-term neonates, 90.3% of preterm neonates at TEA, and 72.9% of preterm neonates before TEA (Table 2). Although capturing only a summary level view, this result suggested that small-world organization is present in a large proportion of neonates

Table 2. The percentages of participants exhibiting strong small-world architecture in the adults and neonate groups.

Groups	$\phi \geq 0.6$		$\sigma \geq 1$	
	Weighted (%)	Binary (%)	Weighted (%)	Binary (%)
Adults	100.0	100.0	92.0	94.3
Full-term neonates	97.8	97.8	83.1	90.3
Preterm neonates at TEA	90.3	94.4	76.4	93.1
Preterm neonates before TEA	72.9	71.4	55.7	74.3

To ensure results' robustness and mitigate the influence of arbitrary data analysis operations, binary and weighted FC matrices were used for graph construction, according to two different algorithms: ϕ (37) and σ (30). A reference value of $\phi \geq 0.6$ or $\sigma \geq 1$ is applied to differentiate a network with a strong vs. weak small-world architecture. PMA, postmenstrual age in weeks; ϕ , small-world propensity calculated according to Muldoon et al. (37); σ , small worldness calculated according to Humphries and Gurney (30).

before TEA, and in the majority/all preterm neonates at TEA/born at full-term age. In the next sections, we performed fine-grained analyses and group comparisons to unravel the effect of prematurity and early infant age on small-world organization.

The effect of premature birth on the development of small-world architecture

When the effects of prematurity and early infant age were collapsed, in the comparison between full-term neonates and

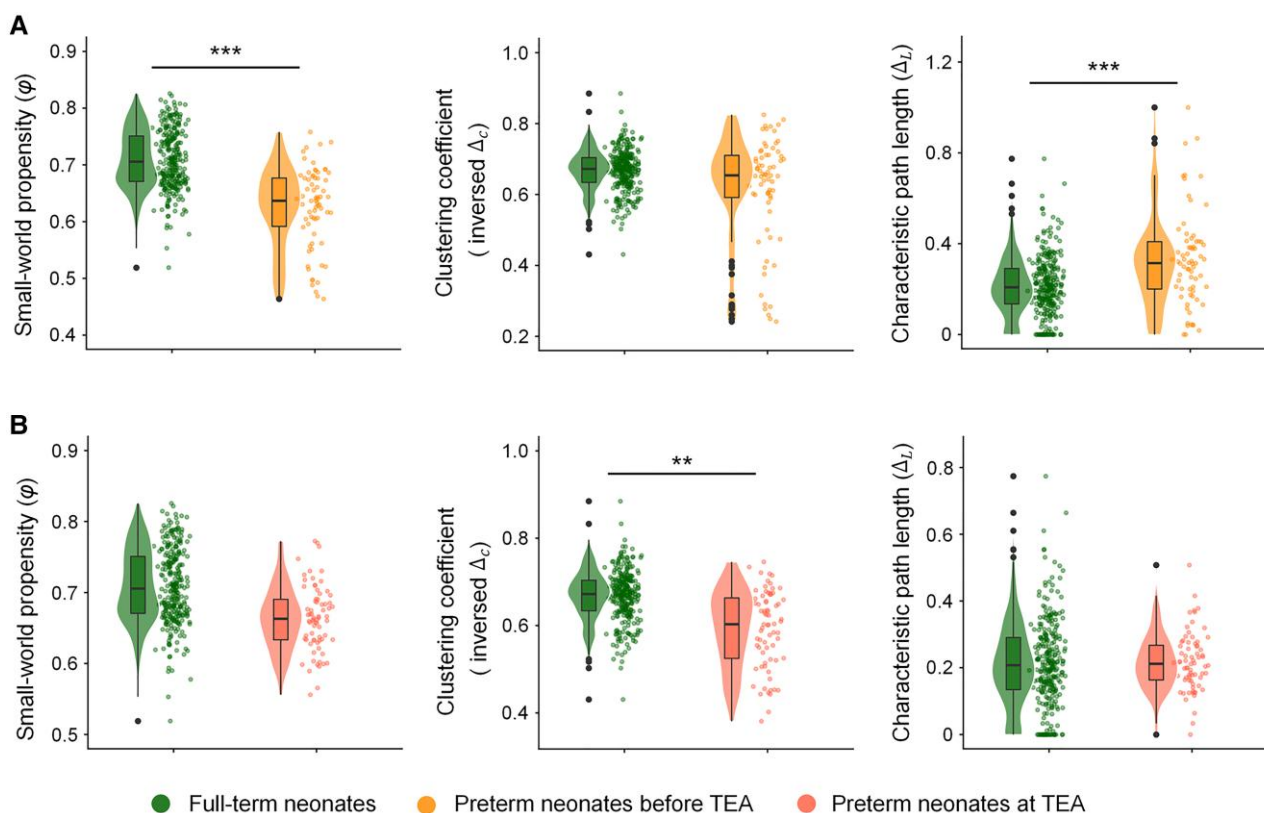


Fig. 2. Effects of premature birth on the development of small-world architecture. A) Small-world properties in the full-term neonates relative to preterm neonates before TEA; B) small-world properties in the full-term neonates relative to preterm neonates at TEA. Full-term neonates had significantly higher small-world propensity and lower normalized path length relative to preterm neonates before TEA, independent of mean FC. Full-term neonates had significantly higher clustering coefficient relative to preterm neonates at TEA. Higher ϕ /inversed Δ_c/Δ_L represent higher small-world propensity, higher clustering coefficient and longer characteristic path length. The inversed Δ_c was calculated by $1 - \Delta_c$ and for visualization purposes only and the statistical analyses were conducted using Δ_c . The violin plots show the distribution of the data. The line that divides the box into two parts represents the median of the data. The ends of the box represent the upper (Q3) and lower (Q1) quartiles of the data. The extreme lines of the boxplot show $Q3 + 1.5 \times$ interquartile to $Q1 - 1.5 \times$ interquartile range. The black dots beyond the extreme lines show potential outliers. TEA, term-equivalent age. *** $P < 0.0005$; ** $P < 0.005$.

preterm neonates before TEA, we found significant main effects of group for ϕ [$F(1, 344) = 86.37, P < 0.0001$] and Δ_L [$F(1, 344) = 43.21, P < 0.0001$], driven by significantly higher ϕ and lower Δ_L in the full-term neonates (Fig. 2A). These results suggested that functional architecture has higher small worldness and higher integration in full-term neonates relative to preterm neonates before TEA at birth.

When the effects of prematurity were considered independently of early infant age, in the comparison between full-term neonates and preterm neonates at TEA, we found a trend main effect of group for ϕ [$F(1, 346) = 5.69, P = 0.018$], driven by higher ϕ in the full-term neonates (Fig. 2B). This result did not survive multiple comparisons correction, and needs to be interpreted with caution. In addition, we observed a significant main effect of group for Δ_c [$F(1, 346) = 10.78, P = 0.001$], driven by a significantly lower Δ_c in full-term neonates relative to preterm neonates at TEA. These results suggested that full-term born neonates had higher segregation than preterm neonates of the same age. Similar findings were observed using different algorithms and types of FC matrices (Fig. S6) and another parcellation (Supplementary material Results, Fig. S8b). These results suggested that, when small-world properties are considered at a fine-grain level, significant effects of prematurity persist when infants reach TEA.

The effect of neonate age on the development of small-world architecture

When we investigated the effect of early infant age, independently of prematurity, by comparing the same preterm neonate group ($n = 33$) that was scanned twice—before and at TEA—we found a significant main effect of neonate age on ϕ [$F(1, 40.21) = 13.23, P = 0.001$], which was driven by significantly higher small-world propensity in preterm at TEA relative to the same group before TEA (Fig. 3B). Similar finding was observed using another brain parcellation (Fig. S9). In addition, we found that the percentage of neonates exhibiting small-world architecture increased from 66.7 to 90.9% when they reached TEA. These results suggested that functional small-world architecture develops significantly with early infant age as premature infants reach TEA.

The effect of premature birth and early infant age on the development of nodal efficiency

The collapsed effects of premature birth and infant age were first considered. The GLMs comparing nodal efficiency between the full-term neonates and preterm neonates before TEA, while controlling mean FC and framewise displacement (FD), showed the full-term neonates had significantly higher nodal efficiency in nine networks: the sensorimotor mouth network (100% of nodes),

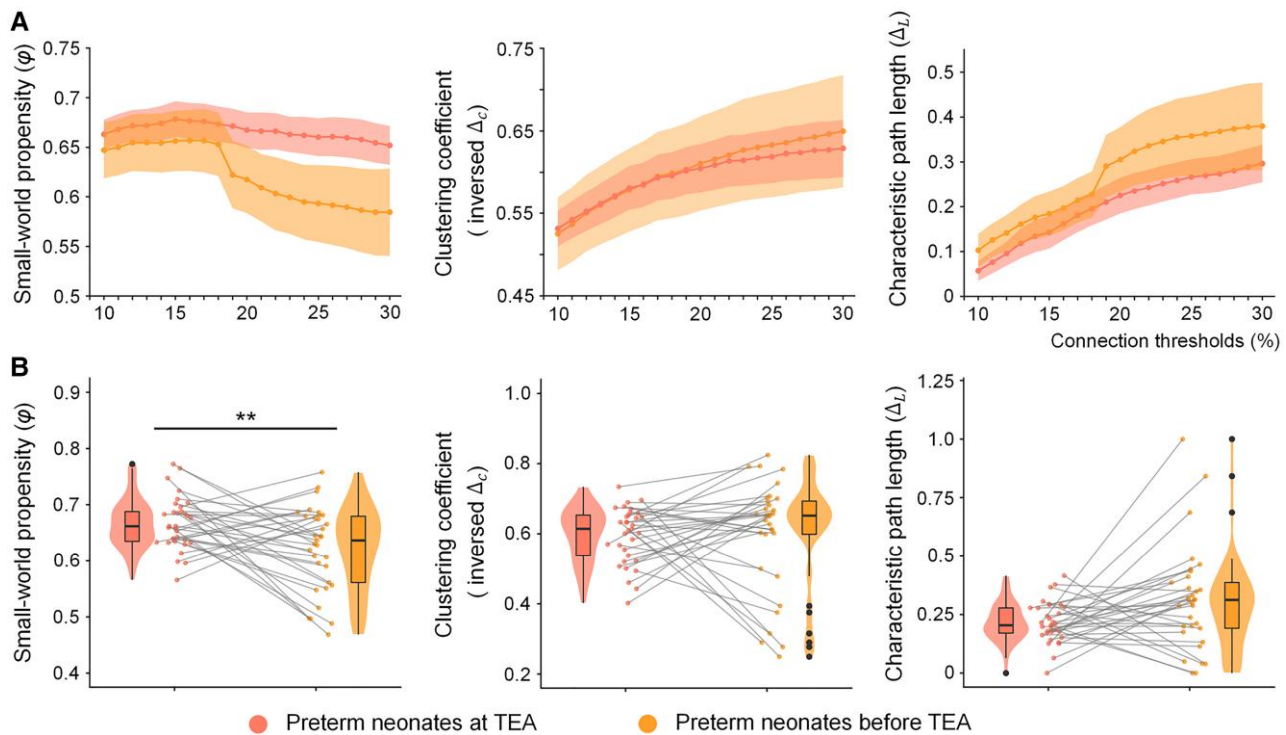


Fig. 3. The development of small-world architecture in preterm neonates up to TEA. A) Small-world properties at all tested thresholds (from 10 to 30% in 1% increments) and B) small-world properties in the preterm neonates at TEA relative to the same neonates scanned before TEA. A) The shaded areas represent the 95% CI. Network properties varied at different thresholds applied. Preterm neonates scanned before TEA showed lower small-world propensity and higher characteristic path length relative to the same neonates scanned at TEA, at 12/21 thresholds. To ensure that results were not driven by a specific choice of thresholds, the small-world propensity, clustering coefficient and characteristic path length were averaged across 21 thresholds prior to statistical analyses. Higher ϕ /inversed Δ_c/Δ_L represent higher small-world propensity, higher clustering coefficient, and longer characteristic path length. The inversed Δ_c was calculated by $1 - \Delta_c$ and for visualization purposes only and the statistical analyses were conducted using Δ_c . B) The violin plots show the distribution of the data. The line that divides the box into two parts represents the median of the data. The ends of the box represent the upper (Q3) and lower (Q1) quartiles of the data. The extreme lines of the boxplot show Q3 + 1.5 * interquartile to Q1 - 1.5 * interquartile range. The black dots beyond the extreme lines show potential outliers. TEA, term-equivalent age. ** $P < 0.005$.

sensorimotor hand network (56.67%), dorsal attention (45.45%), cingular opercular (42.86%), frontoparietal control (41.67%), salience (38.89%), auditory (23.08%), default mode (22.64%), and the visual network (18.52%) (Fig. 4A, Table 3). (Please see [Supplementary material for further supporting results, Figs. S3–S5.](#))

Second, we considered the effect of premature birth independently of infant age. The GLMs comparing nodal efficiency between the full-term neonates and preterm neonates at TEA showed that the full-term neonates had higher nodal efficiency in the right angular gyrus (node 194, frontoparietal control network), the orbital part of right inferior frontal gyrus (node 210, salience network), and the right middle temporal gyrus (node 239, ventral attention network [VAN]) (Fig. 4B). Significant differences in these nodes were also observed relative to preterm neonates before TEA (above; Fig. 4A). Third, when we considered the effect of infant age independently of prematurity, by comparing nodal efficiency between the same preterm neonates scanned before and at TEA, no significant main effects were found (Fig. 4C).

Discussion

In this study, we asked what is the impact of premature birth and early neonate age on the brain's small-world architecture and regional communication efficiency. We found that small-world architecture was developed in full-term born infants. To the best of our knowledge, this is the first fMRI study to investigate

the effect of prematurity before TEA, both on the global small-world properties and the efficiency of regional functional communication. The key finding was that premature neonates before TEA showed significant and widespread differences in small-world brain architecture and in the efficiency of regional communication, relative to full-term born neonates. These differences were driven by both sensory and higher-order networks, with the somatomotor, dorsal attention, cingulo-opercular, and frontoparietal control networks carrying the largest effects, and the visual network the smallest. In addition, we observed that, for the most part, global small-world properties and regional communication efficiency developed in healthy-born premature neonates as they reached TEA, suggesting a preprogrammed developmental trajectory of this functional architecture despite of prematurity. Nevertheless, significant prematurity-related disruption of small-world architecture persisted at TEA.

Comparison of adult and neonate functional architectures

As expected, adults had stronger small-worldness values, including higher clustering coefficient, than all neonate groups, suggesting more efficient and segregated functional brain architecture relative to neonates. It is worth noting that differences in functional architecture between adults and neonate groups, and across neonate groups were independent of any differences in FC or head motion. Importantly, we found that small-world

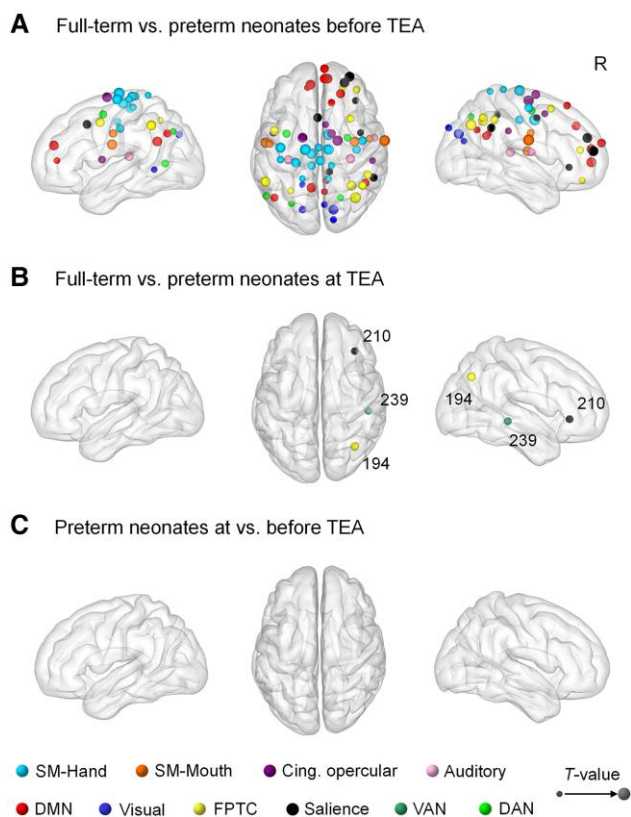


Fig. 4. Effects of premature birth on nodal efficiency. A) Nodes showing higher nodal efficiency in the full-term neonates relative to preterm neonates before TEA; B) nodes showing higher nodal efficiency in the full-term neonates relative to preterm neonates at TEA; and C) no significant difference between preterm neonates scanned at TEA and the same neonates scanned before TEA. The size of the node represents T-value. SM-Hand, sensory/somatomotor hand network; SM-Mouth, sensory/somatomotor mouth network; Cing. opercular, cingulo-opercular task control network; DMN, default mode network; FPTC, frontoparietal task control network; VAN, ventral attention network; DAN, dorsal attention network; R, right.

Table 3. The percentage of nodes showing significantly higher nodal efficiency in each network in the full-term neonates relative to preterm neonates before TEA.

Networks	Percentage of significant nodes
SM-Mouth	100.00% (5/5)
SM-Hand	56.67% (17/30)
DAN	45.45% (5/11)
Cing. Opercular	42.86% (6/14)
FPTC	41.67% (10/24)
Salience	38.89% (7/18)
Auditory	23.08% (3/13)
DMN	22.64% (12/53)
Visual	18.52% (5/27)
Subcortical	0.00% (0/13)
VAN	0.00% (0/9)

SM-Hand, sensory/somatomotor hand network; SM-Mouth, sensory/somatomotor mouth network; Cing. opercular, cingulo-opercular task control network; DMN, default mode network; FPTC, frontoparietal task control network; VAN, ventral attention network; DAN, dorsal attention network.

architecture was developed in full-term born infants. Our findings add robustness to earlier studies in small infant groups, suggesting that small worldness is developed in full-term born neonates (25–29). These results suggest that the functional organization of the brain develops rapidly from birth onwards in the first years

of life, with functional brain networks gradually becoming more cohesive (39, 40) and specialized (29, 41, 42). This is consistent with previous studies using the dHCP dataset (4, 6), which observed actively developing brain networks in full-term neonates from birth onward in the first weeks of life. Eyre et al. (4) found significant expansion of the somatosensory, posterior parietal (core region of the DMN), and visual association networks from 37 to 43.5 weeks in full-term neonates. Connections between regions underwent rewiring, and network architecture changed rapidly during this period (6).

Impact of prematurity and young infant age

A dearth of studies on small-world architecture in premature infants before TEA has led to lack of understanding on the effect of prematurity on small-world organization. The two studies in this area, that these authors are aware of, delivered inconsistent results from small infant cohorts. We address this gap by using the world's largest sample of neonatal functional MRI dataset ($n = 420$) with high temporal and spatial resolution. Our results show that premature neonates before TEA have significantly weaker small-world organization and higher path length, or lower neural integration, relative to full-term neonates. This finding differs from the two previous studies, which reported stronger small-world properties in preterm neonates before TEA (28, 32), a discrepancy likely due to the small sample sizes ($n = 11$ to 23) and the highly specific connectivity parameters (e.g. density 5% threshold) in these previous studies. Furthermore, preterm neonates before TEA showed lower efficiency of regional communication in 32% of 217 nodes, distributed across 9/11 brain networks, relative to full-term counterparts. Lower nodal efficiency was observed both in sensory and higher-order networks. The somatomotor networks showed the most pronounced underdevelopment in nodal efficiency, with those involved in mouth and hand movements showing lower values in 100 and 57% of the relevant nodes, respectively, suggesting that functional communication in these regions undergoes dramatic developments during the third trimester of pregnancy. Fetuses receive somatomotor input from their muscles and limb movements in utero, which is key for early development of movement abilities before birth. Recent work has argued (43) that sensorimotor experience may not only be integral to the development of movement (3) but also to the “core” functions of awareness, to do with body boundaries, position, facial features, visceral states, etc. (44, 45), which are interwoven into the incipient exploratory and increasingly motive- (46) or purpose-driven movement (43) of the developing fetus, by the third trimester. From this perspective, somatomotor brain networks play a critical role for the genesis and evolution of the infant's understanding of their own organism and physical interrelationship with the world. Our results cohere with this idea and suggest that movement of the mouth and hands by birth, and the wider sensorimotor experience supported by the somatomotor brain networks, are key priorities of brain development in the third trimester of pregnancy.

Following closely in the effect of prematurity were networks associated with higher cognition, i.e. the dorsal attention (45% of nodes), cingulo-opercular (43% of nodes), and frontoparietal control (42% of nodes) networks, suggesting that these undergo dramatic development in utero during the third trimester as well, likely to prepare for the rapid development of high-level cognition from birth. This is consistent with our previous findings that prematurity and young infant age significantly impacted the development of the frontoparietal and default mode networks (2). By contrast,

the VAN showed no differences in nodal efficiency between preterms before TEA and full-term neonates, suggesting that regional communication in these networks does not change significantly during the third trimester of pregnancy. As all preterm infants were scanned at or very shortly after birth, these neonates would have had very limited extra-uterine sensory visual experience. The VAN has been implicated in visuospatial cognition (47), and, thus, it likely undergoes experience-dependent changes post birth, once infants are exposed to visual information from their environment. Consistent with this interpretation is the finding the visual network showed reduced efficiency in the fewest nodes (<20%), relative to the other networks in preterm infants before TEA. Taken together, these findings are consistent with the limited visuo-sensory experience of neonates, and suggest that visually driven brain networks develop at a lesser pace than others in the third trimester of pregnancy, and pick up developmental pace post birth, once infants receive continuous visual input. Visual acuity is low in neonates, and it is thought that this period of blurriness plays an adaptive role in enhancing the recognition of fine-grained visual information, as the infant develops (48). The aforementioned features of underdeveloped small-world architecture and regional communication efficiency observed in preterm neonates before TEA are due both to prematurity and young infant age, relative to full-term born neonates.

When infant age was controlled for, in the comparison between preterms at TEA and full-term born neonates, prematurity-related disruptions of small worldness persisted, but at a much lesser extent. This suggested a preprogrammed developmental trajectory of functional architecture despite of prematurity, as infants reach TEA. A recent study by Dall'Orso et al. (3) found that the sensorimotor network develops rapidly as preterm infants reach TEA, with a similar connectivity pattern observed in the sensorimotor network by TEA, as in full-term born neonates.

Nevertheless, we show that preterm neonates at TEA retain significant differences relative to full-term born neonates, specifically significantly smaller clustering coefficient (lower neural segregation), and significantly reduced communication efficiency in 3/217 nodes (i.e. 1.4%, compared to 32% in preterms before TEA). Eyre et al. (4) showed that premature birth was associated with less cohesive brain networks in premature neonates when they reached TEA. We advance the state-of-the-art knowledge on the impact of prematurity on regional communication, by revealing specific regions that show underdevelopment due to prematurity. Particularly, the nodes identified belonged to the salience, visual attention network, and frontoparietal control networks. In addition to partaking in networks that support attention and executive function, these nodes fall within the right angular, inferior frontal gyrus, and middle temporal gyrus, regions that are related to language processing (49–51). Therefore, disruption of nodal efficiency in these regions, associated with prematurity in term-equivalent neonates, may underlie the significant risks for language development delays that are associated with premature birth, such as in language acquisition, word comprehension, and the development of receptive language skills (52–54).

The effect of infant age in and of itself, while controlling for prematurity, was investigated in the comparison of a small subset of preterm neonates ($n = 33$) that were scanned twice, once before TEA and, subsequently, when they reached TEA. As they reached the TEA, these preterm infants showed significantly stronger small-world organization. In addition, the percentage of neonates exhibiting small-world architecture increased from 66.7 to 90.9%,

when they reached TEA. These results suggested that functional small-world architecture develops significantly with early infant age as premature infants reach TEA.

In summary, young premature infants showed the largest and extensive disruption to small-world organization and regional communication efficiency relative to full-term born neonates, underscoring the importance of the third trimester of pregnancy for the development of the brain infrastructure that supports cognition and conscious awareness. This result is consistent with a previously published study (2), where we showed that preterm neonates before TEA did not exhibit distinct high-order networks, particularly the default mode and frontoparietal ECN, in stark contrast to their full-term born counterparts, who manifested these networks as distinct (1) and engaged in the complex antiposed dynamical communication that is observed in the adult brain (2).

Methodological considerations

Although some previous studies have reported a negative association of prematurity with small-world properties (32), others have not (25, 28). This inconsistency is likely due to methodological differences in the type of data acquired, analyses method, small sample sizes, and brain atlases (55) in these previous studies. Here, we were enabled by the high-quality dHCP dataset to employ a uniquely large sample ($n = 420$) of high temporal and spatial resolution infant rs-fMRI data, accurate week-by-week structural templates of the developing infant brain, different graph-theoretical algorithms, and different brain atlases, which ensured higher sensitivity and reproducibility to detect brain functional architecture changes in early infancy. Given these methodological strengths and clear results, we believe this study helps to resolve previous inconsistent findings on the role of prematurity on the development of small-world infrastructure in neonates.

Negative correlations were removed in this study for several reasons: (i) the interpretation of negative connections remains unclear (56). It has been suggested they may be the by-product of preprocessing procedures (particularly global signal regression) and other statistical artifacts, rather than constituting meaningful anticorrelations between brain regions (56–58). (ii) There is no consensus on the best way to model negative correlations (59). (iii) In previous studies, the reliability of graph-theoretical measures was higher when negative correlations were excluded (60). (iv) Negative connections did not survive the stringent FC thresholds (0.1:0.01:0.3), which in this study were used to ensure results were not driven by graph topologies at specific connection densities (61).

We note that the typical development of small worldness may be further delayed or altered in premature infants with birth complications, brain injury or extreme prematurity (i.e. gestational age <28 weeks, very low birth weight <1,500 g), which were not well represented in this study, as has been shown for other markers of high-order cognition (62). Extreme prematurity and clinical conditions related to birth complications could be associated with different functional architectures at TEA, as well as during the preterm period, compared with infants with higher gestational ages, and will be investigated in future studies.

What are the implications of our findings for understanding complex cognition in neonates?

The lack of language and willful motoric output presents major barriers to understanding how and when complex cognition emerges in neonates. These limitations can be sidestepped by

asking a foundational question: whether or not the brain mechanism of complex cognition is present from birth. A feature of this mechanism in adults is small-world brain organization, but its development at birth has, to date, remained poorly understood. For the first time, here we show that by full-term birth or TEA, neonates possess key features of the small-world brain infrastructure that support the integration of information across diverse sensory and higher-order functional modules, which in adults has been found to support high-order cognition (16–20).

These findings significantly advance our understanding of the infant brain and build on recent findings on the development of neuroarchitecture by full-term birth or TEA. For example, Sylvester et al. (1) and Hu et al. (2) found, by full-term birth, the presence of distinct high-order functional brain networks (DMN, ECN, and DAN), and Hu et al. (2) also found the complex interposed dynamics between the DMN and frontoparietal networks, that has been extensively linked to cognition and consciousness in adults (63–65). Linke et al. (7) found that both the ECN and DMN were present even in neonates with perinatal brain injuries, both full-term and preterm neonates scanned at TEA, and that disruption to the ECN at TEA was predictive of the emergence of motor impairments at 4 and 8 months of age, suggesting a causal link between high-order network organization and behavior even at this young infant age. The key novel finding of the present study was that premature neonates before TEA showed dramatic underdevelopment of small-world organization and regional communication in 9/11 networks, with disruption in 32% of brain nodes. Our finding compliments a previous study from the dHCP, reporting that preterm birth was associated with disruption of individual brain networks (4).

In summary, our findings suggest that by birth infants display a neural architecture that has been shown to support complex cognition in healthy adults, and therefore that such capacity may be presents in infants. Recent studies of infant behavior support this conclusion. For example, Mariani et al. (66) found that newborns' electrophysiological activity increased long-range temporal correlations in response to speech they had heard in utero, and Wu et al. (67) found that within 5 h of birth infants learn to discriminate natural vowels from backward vowels, which had only been exposed after birth. Together with these recent findings, our results suggest that newborns are not helpless blank canvases with immature brains entirely unlike those of adults, but rather, that they possess a surprisingly developed proto neuroarchitecture and neural capacity for high-order cognition. Further supporting this conclusion, a recent review (68) suggests that far from being helpless, from birth, human infants are engaged in surprisingly complex learning of a "foundation model": a set of fundamental representations that underpin later cognition with high performance and rapid generalization. Importantly, we also find that small-world organization in neonates is yet to undergo substantial change before it resembles that of the adults, further suggesting that any cognitive experiences are likely limited and rapidly to become more fully fledged as infants develop from the first days and months of life.

Materials and methods

Participants

Neonates

The neonate data were from the second (2019) dHCP public data release (<https://biomedica.github.io/dHCP-release-notes/>). All neonates were scanned at the Evelina Newborn Imaging Centre,

Evelina London Children's Hospital. Ethical approval was obtained from the UK's National Research Ethics Committee, and parental informed consent was obtained before imaging. Neonates were excluded from the dHCP project if they had a history of severe birth complications requiring prolonged resuscitation, a diagnosed chromosomal abnormality, or any contraindications to MRI scanning (such as incompatible implants). Additionally, none of the infants included in the current study required treatment for clinically significant brain injuries. We used 278 full-term neonates (gestational age [GA] at birth = 39.9 weeks \pm 8.6 days; PMA at scan = 41.2 weeks \pm 12.2 days; 119 females) after quality control procedures. Seventy-two scans from the preterm neonates at TEA (GA at birth = 32.1 weeks \pm 25.5 days; PMA at scan = 40.9 weeks \pm 14.6 days; 32 females) and 70 scans from the preterm neonates before TEA (GA at birth = 32.5 weeks \pm 20.7 days; PMA at scan = 34.7 weeks \pm 12.7 days; 22 females) were included after quality control. We also included a subset of paired scans collected from the same preterm infants ($n = 33$, GA at birth = 32.2 weeks \pm 20.1 days) at (PMA at scan = 41.0 weeks \pm 10.16 days) and before TEA (PMA at scan = 34.5 weeks \pm 11.5 days) to investigate the effects of neonate age. Further details on inclusion criteria are shown in Fig. 5 and Table S1.

Adults

As a reference adult group, we used a subset ($n = 176$; 22–36 years; 99 females) of high-quality resting-state functional neuroimaging data from the final release of the Washington University-Minnesota Consortium of Human Connectome Project (HCP) selected by Ito et al. (69). For details of study procedures see Van Essen et al. (70).

Data acquisition and preprocessing

Developing Human Connectome Project

Data were acquired on a 3T Philips Achieva with a dedicated neonatal imaging system including a neonatal 32-channel phased-array head coil. Fifteen minutes of high temporal and spatial resolution rs-fMRI data were acquired using a multislice gradient-echo EPI sequence with multiband excitation (echo time [TE] = 38 ms; repetition time [TR] = 392 ms; multi-band factor = 9 \times ; 2.15 mm isotropic, 2,300 volumes). In addition, single-band EPI reference (sbref) scans were also acquired with bandwidth-matched readout, along with additional spin echo EPI acquisitions with 4xAP and 4xPA phase-encoding directions. To correct susceptibility distortion in rs-fMRI data, field maps were also obtained from an interleaved (dual TE) spoiled gradient-echo sequence (TR = 10 ms; TE1 = 4.6 ms; TE2 = 6.9 ms; flip angle = 10 $^\circ$; 3 mm isotropic in-plane resolution, 6 mm slice thickness). High-resolution T1- and T2-weighted anatomical imaging were also acquired in the same scan session, with a spatial resolution of 0.8 mm isotropic. For T1w image: TR = 4795 ms and the field of view (FOV) = 145 \times 122 \times 100 mm. For T2w image: TR = 12,000 ms, TE = 156 ms and the FOV = 145 \times 122 \times 100 mm.

The preprocessed neonatal rs-fMRI data were provided by the dHCP group. [Please see [Supplementary material Methods](#) and Fitzgibbon et al. (71) for details on the preprocessing pipeline.] In brief, motion and distortion correction and temporal high-pass filter (1/150 Hz high-pass cutoff) procedures were applied. The cardiorespiratory fluctuations and multiband acquisition artifacts, the 24 extended rigid-body motion parameters together with single-subject ICA noise components were regressed out to reduce signal artifacts related to physiological noise and head movement. We then applied intensity normalization to the preprocessed

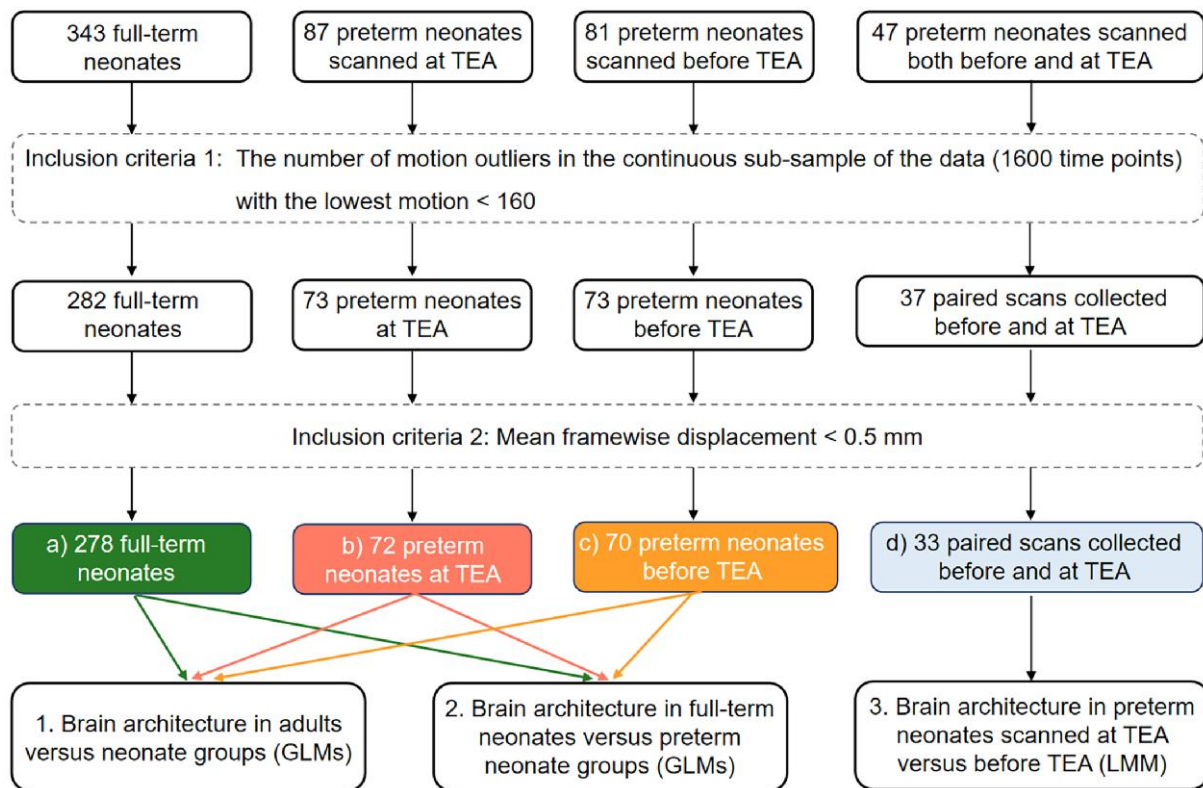


Fig. 5. The number of scans included in data analyses. The frames a), b), and c) indicate the scans collected from full-term neonates/preterm neonates at/before TEA that passed head motion criteria. The frame d) indicates the scans collected at and before TEA from the same preterm neonates. TEA, term-equivalent age; GLMs, general linear models; LMM, linear mixed-effect model.

dHCP rs-fMRI data to keep the preprocessing procedure consistent between neonates and adults. Last, a temporal low-pass filter (0.08 Hz low-pass cutoff) was applied to the neonatal data, as previous studies found that oscillations were primarily detected within gray matter in 0.01–0.08 Hz (72, 73).

To further reduce the effect of motion on graph-theoretical measures, we applied a scrubbing procedure to retain a continuous sub-sample of the data (1,600 time points, ~70%) with the lowest motion for each neonate. Full details of the scrubbing procedure were published in Hu et al. (2). Subjects with more than 160 motion-outlier volumes (10% of the cropped dataset) in the continuous subset were labeled “high level of motion” and excluded entirely. Thus, 61 full-term neonates, 14 preterm neonates scanned at TEA, and 8 preterm neonates scanned before TEA were excluded. In addition, participants whose mean FD after the scrubbing procedure was larger than 0.5 mm were also excluded. Thus, four full-term neonates, one preterm neonate scanned at TEA, and three preterm neonates scanned before TEA were excluded (Fig. 5).

Human Connectome Project

Data were acquired on a customized 3T Siemens “Connectome Skyra” with a 32-channel head coil. Resting-state images were collected using gradient-echo EPI sequence: TR = 720 ms; TE = 33.1 ms; flip angle = 52°; FOV = 208 × 180 mm (readout × phase encoding), slice thickness = 2 mm, 72 slices, 2.0 mm isotropic voxels, 1,200 volumes per run. The HCP rs-fMRI data were preprocessed by the HCP group (74) using the following pipeline: distortion correction, motion correction, alignment of the original rs-fMRI data to the Montreal Neurological Institute (MNI) template space,

intensity normalization, temporal high-pass filter, and denoising using FMRIB’s independent component analysis-based Xnoiseife (ICA-FIX). The detailed preprocessing procedure can be found in [Supplementary material Methods section](#). Then, we applied a temporal low-pass filter (0.08 Hz low-pass cutoff) to the preprocessed adult data.

As the subset of HCP data had controlled head motion (i.e. exclusion of participants that had any fMRI run in which more than 50% of TRs had greater than 0.25 mm FD), and adults generally have smaller maximal head motion than neonates, we did not apply the same scrubbing method used in the dHCP dataset to adult data. In addition, we randomly chose a continuous sub-sample of data time-series (871 time points) in adults as in neonates.

Data analyses

Node definition

Using a meta-analytically derived functional brain atlas from Power et al. (75), we defined 264 cortical and subcortical regions of interest (ROIs) (8-mm radius spheres) in MNI space. 33 uncertain nodes (do not belong to any of the 11 networks) and 5 cerebellar nodes were excluded. Therefore, we included the remaining 226 nodes comprised 11 networks according to the network labels provided by Power et al. (75): (i) sensory/somatomotor hand (30 nodes), (ii) sensory/somatomotor mouth (5 nodes), (iii) cingulo-opercular control (14 nodes), (iv) auditory (13 nodes), (v) default mode (57 nodes), (vi) visual (31 nodes); (vii) frontoparietal control (25 nodes), (viii) salience (18 nodes), (ix) subcortical (13 nodes), (x) ventral attention (9 nodes), and (xi) dorsal attention (11 nodes) networks. For neonates, the 226 ROIs in MNI space

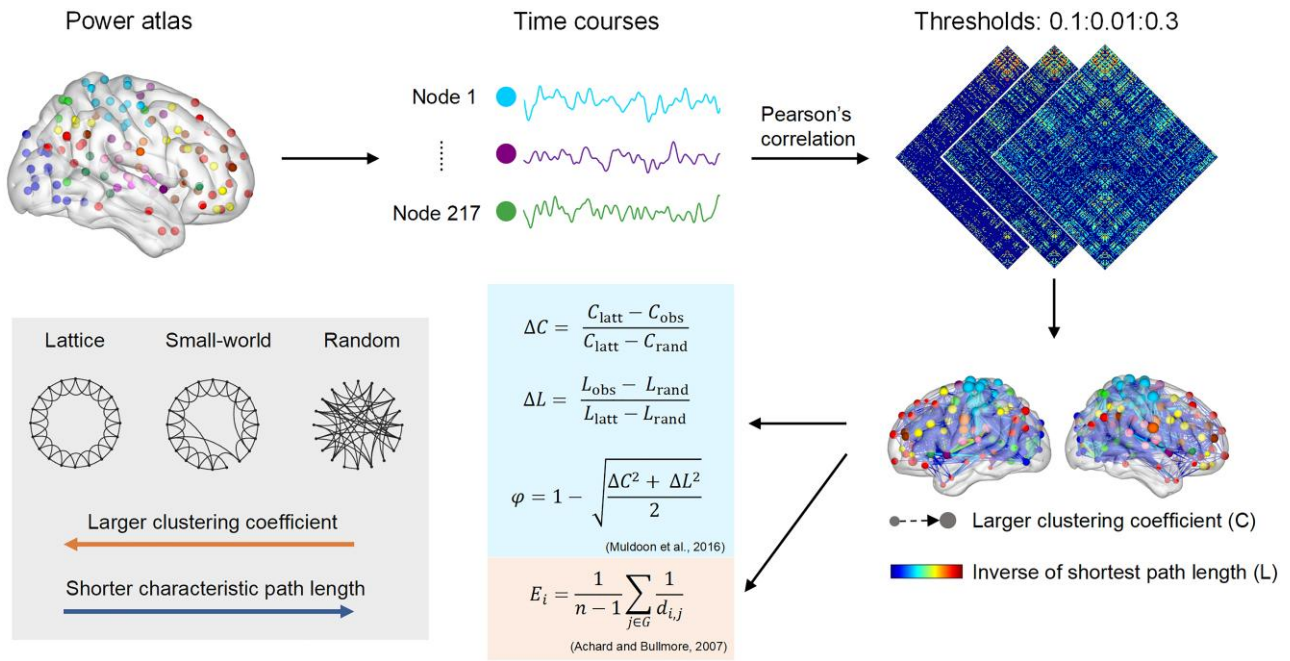


Fig. 6. Schematic of the method. Time courses were extracted from each brain node, and Pearson's correlation was applied to obtain a weighted graph for each participant. Twenty-one proportional thresholds from 10 to 30% in 1% increments were applied to threshold the weighted graphs. The local clustering coefficient for each node and the shortest path length between every two nodes were calculated based on weighted graphs at each cost function. Nodal efficiency for each node was calculated based on shorted path length at each cost function and then averaged (38). Then, small-world propensity, normalized clustering coefficient, and normalized characteristic path length for each brain network were calculated at each cost function and averaged (37).

were transformed into neonate native space using the following two-step procedure. We first aligned the ROIs in MNI space with the 40-week dHCP T1w template (76) using the warp file generated from the transformation between the MNI T1w template and 40-week dHCP T1w template using advanced normalization tools (see [Supplementary material Methods](#) for details). Then, the nodes in 40-week dHCP T1w template space were transformed into neonate native space by applying the inverted func-to-template warp provided by the dHCP group (71) using FMRIB software library. Time courses were extracted from each neonate based on these ROIs in native space and from adults based on ROIs in the MNI space.

To ensure the same number of nodes/connections across groups, in the following graph construction, the extracted time courses from adults, full-term neonates, preterm neonates at TEA, and preterm neonates before TEA underwent rigorous inspection. Nine nodes were further excluded because of low registration accuracy according to the following criteria: (i) over 5% of participants in any of the four groups missed time courses in that node; (ii) node showed significant differences in the proportions of participants having missing time courses between the four groups. Thus, four nodes of DMN (nodes 83, 116, 119, and 120), four nodes of the visual network (nodes 153, 165, 168, and 172), and node 179 of the frontoparietal control network were excluded (Fig. S10).

Graph construction

The Pearson's correlation between time courses of any two pairs of nodes was calculated. Then, self-connections were set to 0, and NaNs and negative correlations were removed. Twenty-one proportional thresholds, from 10 to 30% in 1% increments (77, 78), were used to threshold functional matrices (Fig. 6) to ensure

that results were not driven by specific connection densities (59, 61, 79). Weighted graphs retain more biologically relevant information relative to their binary graphs (9, 61, 80) and were used here in addition to binary ones.

Small-world properties

Nodal-level clustering coefficient and shortest path length were first calculated based on the FC matrices under each threshold for each participant. The clustering coefficient of a node captures the tendency to which the neighboring nodes of a node are interconnected (81), and it was computed as follows (82)

$$C_i = \frac{1}{k_i(k_i - 1)} \sum_{j,k} (\hat{w}_{ij} \hat{w}_{jk} \hat{w}_{ik})^{1/3}, \quad (1)$$

where C_i corresponds to the clustering coefficient of node i , k_i is the number of edges connected to node i , w_{ij} corresponds to the strength of a connection between nodes i and j , and \hat{w}_{ij} represents the weight scaled by the highest weight in the network ($\hat{w}_{ij} = w_{ij}/\max(w)$). Then, the global-level clustering coefficient was calculated by averaging the nodal-level clustering coefficient across all nodes.

The shortest path length represents the lowest cost of information moving between them. Thus, for weighted FC matrices, the nodal-level shortest path length is defined as

$$d_{ij} = 1/w_{ij}. \quad (2)$$

The global-level characteristic path length is given by (83).

$$L = \frac{1}{N(N-1)} \sum_{i \neq j} d_{ij}. \quad (3)$$

The commonly used formula to quantify small worldness proposed by Humphries and Gurney (30) (see [Supplementary](#)

material Methods for detailed description) has been criticized (9, 11, 31), because it is strongly driven by network clustering and density of the graph. Telesford et al. (31) established a new small-worldness index separately comparing network clustering to a regular network and path length to a random network. In the present study, an alternative index (ϕ) proposed by Muldoon et al. (37) was used to investigate whether or not neonates' brains at birth show a similar functional small-world architecture to the adult brain. This follows Telesford et al.'s measure (31) and, at the same time, takes variations in network density and connection strengths into account. The ϕ is computed according to the following equation

$$\phi = 1 - \sqrt{\frac{\Delta_C^2 + \Delta_L^2}{2}}, \quad (4)$$

where

$$\Delta_C = \frac{C_{\text{latt}} - C_{\text{obs}}}{C_{\text{latt}} - C_{\text{rand}}} \quad (5)$$

and

$$\Delta_L = \frac{L_{\text{obs}} - L_{\text{rand}}}{L_{\text{latt}} - L_{\text{rand}}}, \quad (6)$$

where latt/obs/rand represent lattice/observed/random networks, the Δ_C and Δ_L represent the fractional deviation of the C_{obs} or L_{obs} from its respective lattice and random networks constructed with the same number of nodes and the same degree distribution (null model). Thus, Δ_C and Δ_L both range from 0 to 1, and a higher value means the observed networks have a lower clustering coefficient and a higher characteristic path length. The ϕ ranges from 0 to 1, and a higher ϕ value reflects the observed networks exhibiting stronger small-world architecture.

The normalized small-world properties, Δ_C , Δ_L , and ϕ , were then averaged across all 21 thresholds for further statistical analyses. In addition, we also calculated the mean strength of FC, which can be a confound in between-group difference of small-world properties (79). The mean FC was calculated for each participant by averaging all positive edges.

Nodal efficiency

To quantify the communication efficiency at individual brain node, we used nodal efficiency (E_i), which is defined as follows (38):

$$E_i = \frac{1}{n-1} \sum_{j \in G} \frac{1}{d_{ij}}, \quad (7)$$

where E_i is the mean of the inverse shortest path length from node i to the other nodes. Brain node having high E_i exhibits a high level of efficiency in communicating with the rest of the brain.

Statistical analyses

Comparison in functional brain architecture at the global level

Adults vs. neonates

To investigate how the functional brain architecture in neonates differs from that of adults, we compared small-world properties in the adults and neonate groups. GLMs were used to test the difference in ϕ , normalized clustering coefficient (Δ_C), or normalized characteristic path length (Δ_L) between adults and each neonate group while controlling for mean FD and FC, which are significantly different between the adults and neonate groups (Figs. S1 and S2a).

Full-term vs. preterm neonates

To investigate the effect of premature birth on the development of functional architecture at the global level, we compared the normalized small-world properties (ϕ , Δ_C , and Δ_L) between the full-term neonates and preterm neonates at/before TEA. GLMs were used to detect the difference between full-term neonates and preterm neonates at or before TEA while controlling for mean FD and FC.

Preterm neonates scanned at TEA vs. preterm neonates before TEA

A smaller sample of 33 preterm neonates scanned both before and at TEA was used to investigate how small-world architecture develops in preterm neonates from before to reaching TEA. Linear mixed-effect models were applied to detect the difference in small-world properties (ϕ , Δ_C , or Δ_L) between preterm neonates scanned at and before TEA while controlling for mean FD and FC.

Comparison in nodal efficiency between full-term and preterm neonates

To investigate the effect of premature birth on efficiency of regional communication, GLMs were used to detect any differences in nodal efficiency between full-term neonates and preterm neonates at or before TEA, while controlling for mean FD and FC. Correction for the false discovery rate was applied to all statistical results at a threshold of $P < 0.05$.

Validation analyses

The main global-level network analyses in the current study were based on weighted FC matrices and the algorithms proposed by Muldoon et al. (37) (see [Supplementary material Methods](#) for details on definition and algorithms). To ensure that our results were not driven by specific choice of network types and algorithms, we also calculated and compared small-world architecture using (i) binary FC matrices and algorithms proposed by Muldoon et al. (37); (ii) weighted FC matrices and algorithms proposed by Humphries and Gurney (30); and (iii) binary FC matrices and algorithms proposed by Humphries and Gurney (30). In addition, given how graph-theoretical analysis results may be driven by specific parcellations, we tested the reproducibility of our results using another parcellation, the UNC-0-1-2 atlas with 223 regions (84), as a recent study (85) showed a parcellation with about 200 regions may be the most representative for functional network (see [Supplementary material Methods](#) for details on node definition).

Supplementary Material

[Supplementary material](#) is available at *PNAS Nexus* online.

Funding

Neonate data were provided by the Developing Human Connectome Project (<https://www.developingconnectome.org/>), KCL-Imperial-Oxford Consortium funded by the European Research Council under the European Union Seventh Framework Programme (FP/2007-2013)/ERC grant agreement no. [319456]. We are grateful to the families who generously supported this trial. Adult data were provided [in part] by the Human Connectome Project (<http://www.humanconnectomeproject.org/>), WU-Minn Consortium (Principal Investigators: David Van Essen and Kamil Ugurbil (

adult/document/hcp-citations); 1U54MH091657) funded by the 16 NIH Institutes and Centers that support the NIH Blueprint for Neuroscience Research; and by the McDonnell Center for Systems Neuroscience at Washington University. H.H. was funded by the China Scholarship Council—Trinity College Dublin Joint Scholarship Programme (<https://www.tcd.ie/study/international/scholarships/postgraduate/csc/>). E.A.S. was funded by Queens' College, Cambridge Stephen Erskine Fellowship, and the Canadian Institute for Advanced Research. L.N. was funded by an L'Oreal for Women In Science International Rising Talent Award, and the Wellcome Trust Institutional Strategic Support Fund.

Author Contributions

Study conceptualization: L.N. and H.H.; Methodology: H.H., P.C., and L.N.; Formal analyses: H.H.; Writing: H.H. and L.N.; Revision: P.C., E.A.S., and L.N.; Funding and resource acquisition: L.N.; Project administration: L.N.; Supervision, L.N.

Preprints

This manuscript was posted on a preprint: <https://doi.org/10.1101/2023.06.12.544595>.

Data Availability

The neonate data used in the current study were provided by the dHCP (<https://www.developingconnectome.org/>) (71). Adult data were provided [in part] by the HCP (<http://www.humanconnectomeproject.org/>) (69). The graph theory analysis was based on the Brain Connectivity Toolbox (<https://sites.google.com/site/bctnet/>) and SWP (<https://complexsystems.upenn.com/codedata>). The code is available on GitHub (https://github.com/huiqinghu/Graph-theory_Infant-project.git).

References

- Sylvester CM, et al. 2023. Network-specific selectivity of functional connections in the neonatal brain. *Cereb Cortex*. 33:2200–2214.
- Hu H, Cusack R, Naci L. 2022. Typical and disrupted brain circuitry for conscious awareness in full-term and preterm infants. *Brain Commun*. 4:fcac071.
- Dall'Orso S, et al. 2022. Development of functional organization within the sensorimotor network across the perinatal period. *Hum Brain Mapp*. 43:2249–2261.
- Eyre M, et al. 2021. The developing human connectome project: typical and disrupted perinatal functional connectivity. *Brain*. 144:2199–2213.
- Vanes L, et al. 2023. Longitudinal neonatal brain development and socio-demographic correlates of infant outcomes following preterm birth. *Dev Cogn Neurosci*. 61:101250.
- Fenn-Moltu S, et al. 2023. Development of neonatal brain functional centrality and alterations associated with preterm birth. *Cereb Cortex*. 33:5585–5596.
- Linke AC, et al. 2018. Disruption to functional networks in neonates with perinatal brain injury predicts motor skills at 8 months. *NeuroImage Clin*. 18:399–406.
- Bassett DS, Bullmore E. 2006. Small-world brain networks. *Neuroscientist*. 12:512–523.
- Bassett DS, Bullmore ET. 2017. Small-World brain networks revisited. *Neuroscientist*. 23:499–516.
- Liao X, Vasilakos AV, He Y. 2017. Small-world human brain networks: perspectives and challenges. *Neurosci Biobehav Rev*. 77:286–300.
- Papo D, Zanin M, Martínez JH, Buldú JM. 2016. Beware of the small-world neuroscientist! *front. Hum Neurosci*. 10:96.
- Takagi K. 2019. Principles of mutual information maximization and energy minimization affect the activation patterns of large scale networks in the brain. *Front Comput Neurosci*. 13:86.
- Takagi K. 2018. Information-Based principle induces small-world topology and self-organized criticality in a large scale brain network. *Front Comput Neurosci*. 12:65.
- Tan TL, Cheong SA. 2017. Statistical complexity is maximized in a small-world brain. *PLoS One*. 12:e0183918.
- Valencia M., Martinerie J., Dupont S., Chavez M. 2008. Dynamic small-world behavior in functional brain networks unveiled by an event-related networks approach. *Phys Rev E Stat Nonlin Soft Matter Phys*. 77:050905.
- Ginestet CE, Simmons A. 2011. Statistical parametric network analysis of functional connectivity dynamics during a working memory task. *Neuroimage*. 55:688–704.
- Langer N, et al. 2012. Functional brain network efficiency predicts intelligence. *Hum Brain Mapp*. 33:1393–1406.
- van den Heuvel MP, Stam CJ, Kahn RS, Hulshoff Pol HE. 2009. Efficiency of functional brain networks and intellectual performance. *J Neurosci*. 29:7619–7624.
- Douw L, et al. 2011. Cognition is related to resting-state small-world network topology: an magnetoencephalographic study. *Neuroscience*. 175:169–177.
- Wang L, Li Y, Metzack P, He Y, Woodward TS. 2010. Age-related changes in topological patterns of large-scale brain functional networks during memory encoding and recognition. *Neuroimage*. 50:862–872.
- Luppi AI, et al. 2021. Brain network integration dynamics are associated with loss and recovery of consciousness induced by sevoflurane. *Hum Brain Mapp*. 42:2802–2822.
- Barttfeld P, et al. 2015. Signature of consciousness in the dynamics of resting-state brain activity. *Proc Natl Acad Sci U S A*. 112:887–892.
- Duclos C, et al. 2021. Brain network motifs are markers of loss and recovery of consciousness. *Sci Rep*. 11:3892.
- Luppi AI, et al. 2019. Consciousness-specific dynamic interactions of brain integration and functional diversity. *Nat Commun*. 10:4616.
- Bouyssi-Kobar M, et al. 2019. Altered functional brain network integration, segregation, and modularity in infants born very preterm at term-equivalent age. *J Pediatr*. 213:13–21.e1.
- Gozdas E, et al. 2018. Altered functional network connectivity in preterm infants: antecedents of cognitive and motor impairments? *Brain Struct Funct*. 223:3665–3680.
- De Asis-Cruz J, Bouyssi-Kobar M, Evangelou I, Vezina G, Limperopoulos C. 2015. Functional properties of resting state networks in healthy full-term newborns. *Sci Rep*. 5:17755.
- Omidvarnia A, Fransson P, Metsäranta M, Vanhatalo S. 2014. Functional bimodality in the brain networks of preterm and term human newborns. *Cereb Cortex*. 24:2657–2668.
- Fransson P, Åden U, Blennow M, Lagercrantz H. 2011. The functional architecture of the infant brain as revealed by resting-state fMRI. *Cereb Cortex*. 21:145–154.
- Humphries MD, Gurney K. 2008. Network 'small-world-ness': a quantitative method for determining canonical network equivalence. *PLoS One*. 3:e0002051.

- 31 Telesford QK, Joyce KE, Hayasaka S, Burdette JH, Laurienti PJ. 2011. The ubiquity of small-world networks. *Brain Connect.* 1: 367–375.
- 32 Cao M, et al. 2017. Early development of functional network segregation revealed by connectomic analysis of the preterm human brain. *Cereb Cortex.* 27:1949–1963.
- 33 Doria V, et al. 2010. Emergence of resting state networks in the preterm human brain. *Proc Natl Acad Sci U S A.* 107:20015–20020.
- 34 Allievi AG, et al. 2016. Maturation of sensori-motor functional responses in the preterm brain. *Cereb. Cortex.* 26:402–413.
- 35 Zhang H, Shen DG, Lin WL. 2019. Resting-state functional MRI studies on infant brains: a decade of gap-filling efforts. *Neuroimage.* 185:664–684.
- 36 Bhutta AT, Cleves MA, Casey PH, Craddock MM, Anand KJS. 2002. Cognitive and behavioral outcomes of school-aged children who were born preterm—a meta-analysis. *JAMA.* 288:728–737.
- 37 Muldoon SF, Bridgeford EW, Bassett DS. 2016. Small-world propensity and weighted brain networks. *Sci Rep.* 6:22057.
- 38 Achard S, Bullmore E. 2007. Efficiency and cost of economical brain functional networks. *PLoS Comput Biol.* 3:e17.
- 39 Sherman LE, et al. 2014. Development of the default mode and central executive networks across early adolescence: a longitudinal study. *Dev Cogn Neurosci.* 10:148–159.
- 40 Gao W, et al. 2009. Evidence on the emergence of the brain's default network from 2-week-old to 2-year-old healthy pediatric subjects. *Proc Natl Acad Sci U S A.* 106:6790–6795.
- 41 Wen X, et al. 2019. First-year development of modules and hubs in infant brain functional networks. *Neuroimage.* 185:222–235.
- 42 Scheinost D, et al. 2016. Preterm birth alters neonatal, functional rich club organization. *Brain Struct Funct.* 221:3211–3222.
- 43 Delafield-Butt J, Ciaunica A. 2024. Sensorimotor foundations of self-consciousness in utero. *Curr Opin Behav Sci.* 59:101428.
- 44 Damasio Antonio R. 2000. A neurobiology for consciousness. In: Metzinger T, editor. *Neural correlates of consciousness: empirical and conceptual questions.* London: The MIT Press. p. 111–120.
- 45 Sturm VE, Hua AY, Rosen HJ. 2018. Self-awareness and frontal lobe networks. In: Miller BL, Cummings JL, editors. *The human frontal lobes: functions and disorders.* 3rd ed. New York: The Guilford Press. p. 171–183.
- 46 Trevarthen C, Aitken KJ. 2001. Infant intersubjectivity: research, theory, and clinical applications. *J Child Psychol Psychiatry.* 42: 3–48.
- 47 Corbetta M, Shulman GL. 2002. Control of goal-directed and stimulus-driven attention in the brain. *Nat Rev Neurosci.* 3: 201–215.
- 48 Vogelsang L, et al. 2018. Potential downside of high initial visual acuity. *Proc Natl Acad Sci U S A.* 115:11333–11338.
- 49 Friederici AD. 2011. The brain basis of language processing: from structure to function. *Physiol Rev.* 91:1357–1392.
- 50 Perani D, et al. 2011. Neural language networks at birth. *Proc Natl Acad Sci U S A.* 108:16056–16061.
- 51 Hickok G, Poeppel D. 2007. The cortical organization of speech processing. *Nat Rev Neurosci.* 8:393–402.
- 52 Vandormael C, Schoenhals L, Hüppi PS, Filippa M, Borradori Tolsa C. 2019. Language in preterm born children: atypical development and effects of early interventions on neuroplasticity. *Neural Plast.* 2019:6873270.
- 53 Rushe TM. 2010. Language function after preterm birth. In: Nosarti C, Murray RM, Hack M, editors. *Neurodevelopmental outcomes of preterm birth.* Cambridge: Cambridge University Press. p. 176–184.
- 54 Guarini A, et al. 2009. Reconsidering the impact of preterm birth on language outcome. *Early Hum Dev.* 85:639–645.
- 55 Coppola P, et al. 2022. Network dynamics scale with levels of awareness. *Neuroimage.* 254:119128.
- 56 Murphy K, Fox MD. 2017. Towards a consensus regarding global signal regression for resting state functional connectivity MRI. *Neuroimage.* 154:169–173.
- 57 Murphy K, Birn RM, Handwerker DA, Jones TB, Bandettini PA. 2009. The impact of global signal regression on resting state correlations: are anti-correlated networks introduced? *Neuroimage.* 44:893–905.
- 58 Saad ZS, et al. 2012. Trouble at rest: how correlation patterns and group differences become distorted after global signal regression. *Brain Connect.* 2:25–32.
- 59 Hallquist MN, Hillary FG. 2018. Graph theory approaches to functional network organization in brain disorders: a critique for a brave new small-world. *Netw Neurosci.* 3:1–26.
- 60 Wang J-H, et al. 2011. Graph theoretical analysis of functional brain networks: test-retest evaluation on short-and long-term resting-state functional MRI data. *PLoS One.* 6:e21976.
- 61 Rubinov M, Sporns O. 2010. Complex network measures of brain connectivity: uses and interpretations. *Neuroimage.* 52:1059–1069.
- 62 Emberson LL, Boldin AM, Riccio JE, Guillet R, Aslin RN. 2017. Deficits in top-down sensory prediction in infants at risk due to premature birth. *Curr Biol.* 27:431–436.
- 63 Huang Z, Zhang J, Wu J, Mashour GA, Hudetz AG. 2020. Temporal circuit of macroscale dynamic brain activity supports human consciousness. *Sci Adv.* 6:eaaz0087.
- 64 Haugg A, et al. 2018. Do patients thought to lack consciousness retain the capacity for internal as well as external awareness? *Front Neurol.* 9:492.
- 65 Bonhomme V, Boveroux P, Brichant JF, Laureys S, Boly M. 2012. Neural correlates of consciousness during general anesthesia using functional magnetic resonance imaging (fMRI). *Arch Ital Biol.* 150:155–163.
- 66 Mariani B, et al. 2023. Prenatal experience with language shapes the brain. *Sci Adv.* 9:eadj3524.
- 67 Wu YJ, et al. 2022. Rapid learning of a phonemic discrimination in the first hours of life. *Nat Hum Behav.* 6:1169–1179.
- 68 Cusack R, Ranzato M, Charvet CJ. 2024. Helpless infants are learning a foundation model. *Trends Cogn Sci.* 28:726–738.
- 69 Ito T, et al. 2020. Task-evoked activity quenches neural correlations and variability across cortical areas. *PLoS Comput Biol.* 16: e1007983.
- 70 Van Essen DC, et al. 2013. The WU-Minn Human Connectome Project: an overview. *Neuroimage.* 80:62–79.
- 71 Fitzgibbon SP, et al. 2020. The developing Human Connectome Project (dHCP) automated resting-state functional processing framework for newborn infants. *Neuroimage.* 223:117303.
- 72 Zuo XN, et al. 2010. The oscillating brain: complex and reliable. *Neuroimage.* 49:1432–1445.
- 73 Salvador R, et al. 2008. A simple view of the brain through a frequency-specific functional connectivity measure. *Neuroimage.* 39:279–289.
- 74 Glasser MF, et al. 2013. The minimal preprocessing pipelines for the human connectome project. *Neuroimage.* 80:105–124.
- 75 Power JD, et al. 2011. Functional network organization of the human brain. *Neuron.* 72:665–678.
- 76 Schuh, A, et al. 2018. Unbiased construction of a temporally consistent morphological atlas of neonatal brain development. *BioRxiv* 251512. <https://doi.org/10.1101/251512>, preprint: not peer reviewed.
- 77 Godwin D, Barry RL, Marois R. 2015. Breakdown of the brain's functional network modularity with awareness. *Proc Natl Acad Sci U S A.* 112:3799–3804.

-
- 78 Monti MM, et al. 2013. Dynamic change of global and local information processing in propofol-induced loss and recovery of consciousness. *PLoS Comput Biol.* 9:e1003271.
- 79 van den Heuvel MP, et al. 2017. Proportional thresholding in resting-state fMRI functional connectivity networks and consequences for patient-control connectome studies: issues and recommendations. *Neuroimage.* 152:437–449.
- 80 Bolaños M, Bernat EM, He B, Aviyente S. 2013. A weighted small world network measure for assessing functional connectivity. *J Neurosci Methods.* 212:133–142.
- 81 Watts DJ, Strogatz SH. 1998. Collective dynamics of ‘small-world’ networks. *Nature.* 393:440–442.
- 82 Onnela J-P, Saramäki J, Kertész J, Kaski K. 2005. Intensity and coherence of motifs in weighted complex networks. *Phys Rev E.* 71:065103.
- 83 Percha B, Dzakpasu R, Żochowski M, Parent J. 2005. Transition from local to global phase synchrony in small world neural network and its possible implications for epilepsy. *Phys Rev E Stat Nonlin Soft Matter Phys.* 72:031909.
- 84 Shi F, Salzwedel AP, Lin W, Gilmore JH, Gao W. 2018. Functional brain parcellations of the infant brain and the associated developmental trends. *Cereb Cortex.* 28:1358–1368.
- 85 Luppi AI, Stamatakis EA. 2021. Combining network topology and information theory to construct representative brain networks. *Netw Neurosci.* 5:96–124.